Spherical particle immersed in a nematic liquid crystal: Effects of confinement on the director field configurations

S. Grollau, N. L. Abbott, and J. J. de Pablo
Department of Chemical Engineering, University of Wisconsin, 1415 Engineering Drive, Madison, Wisconsin 53706
(Received 25 June 2002; published 16 January 2003)

The effects of confinement on the director field configurations are studied for a spherical particle immersed in a nematic liquid crystal. The liquid crystal is confined in a cylindrical geometry and the particle is located on the axis of symmetry. A finite element method is used to minimize the Frank free energy for various sizes of the system. The liquid crystal is assumed to possess strong anchoring at all the surfaces in the system. Two structures are examined for strong homeotropic anchoring at the surface of the particle: configuration with a Saturn ring disclination line and configuration with a satellite point defect (hedgehog defect). It is shown that the equilibrium locations of the Saturn ring and of the hedgehog point defect change with confinement. It is also found that confinement induces an increase in the elastic free energy that differs substantially with the type of topological defect under consideration. In particular, the evaluation of the total free energy that includes an approximate contribution for the core defect shows that, for micrometer-sized particles in confined systems, the Saturn ring configuration appears to be more stable than the hedgehog defect. This result is in contrast to the bulk situation, where the hedgehog is more stable than the Saturn ring, and it helps explain recent experimental observations of Saturn ring defects around confined micrometer-sized solid particles.

DOI: 10.1103/PhysRevE.67.011702 PACS number(s): 61.30.Jf, 77.84.Nh, 64.70.Md, 61.30.Dk

I. INTRODUCTION

Colloidal suspensions and emulsions have attracted considerable attention in technology and condensed matter physics. Colloidal systems or emulsions in a host liquid crystalline fluid are of particular interest [1,2]. Several past experimental studies have reported that the introduction of isotropic liquid microdroplets into uniformly aligned nematic liquid crystals is accompanied by the formation of topological defects around the droplets. The topological defects appear to mediate anisotropic forces that act between the droplets and lead to the formation of unusual microstructures [3], such as linear chains. These anisotropic forces have been the subject of theoretical studies [4–6] and also of direct experimental measurements [7]. As shown in these studies, the nature of the forces between spherical colloids depends on the symmetry of the director configuration and also on the particle position with respect to the director axis [4]. Topological defects can also mediate interactions with confining surfaces. For a quadrupolar spherical colloid, theoretical arguments have been used [6] to determine the profile of the director at a distance remote from the particle, indicating that the interaction between the particle with confining surfaces is repulsive for a rigidly anchored surface and is attractive at short separation distances if the sample surface exhibits soft anchoring.

Distortions yielding topological defects can be induced by the geometry of the system and by controlling the orientation of the liquid crystal at various surfaces in the system (the so-called anchoring conditions). At the experimental level, various treatments of solid surfaces such as mechanical rubbing [8] or chemisorption of alkanethiols [9] permit control of molecular orientation at the surfaces. For a water droplet in a liquid crystal, the anchoring conditions may be controlled by using various amphiphilic compounds adsorbed at the droplet-liquid crystal interface [2]. Parallel and perpendicular orientations at a surface are referred to as planar and homeotropic anchoring, respectively. In the bulk, insertion of a spherical particle into a nematic solvent with strong homeotropic anchoring at its surface yields two possible director configurations: configuration with a Saturn ring disclination line or configuration with a satellite point defect (hedgehog defect). Determining the director distribution for each of these defects has been the subject of a number of studies. Some authors have proposed models based on the analogy between the director **n** and an electrostatic field [1,3]. Theoretical studies [4,10] have investigated the effect of the strength of anchoring at the surface of the particle on the director configuration. The director configuration around a spherical particle has also been studied using molecular dynamics [11], by numerical minimization of the Frank free energy [12] and by Monte Carlo simulations [13]. Most studies of particles dispersed in nematic fluids have been largely concentrated on bulk systems. Experimental studies of the effects of confining surfaces on such systems have been limited and, to the best of our knowledge, corresponding theoretical or numerical analyses have not appeared in the literature. Studies of bulk systems by Stark [12] have shown that the Saturn ring is favored as the size of the particle is decreased, and also by the application of an external magnetic field. Literature results indicate that micrometer particles in the bulk are accompanied by a hedgehog defect, consistent with experimental observations [2]. In this paper, we present a numerical investigation of the effects of confining surfaces on the director field configurations around a spherical particle that exhibits strong homeotropic anchoring at its surface.

The effect of the confinement on the isotropic-nematic transition has been intensively investigated both experimentally [14,15] and theoretically [16–18]. The preferred orientation of the molecules at a confining surface produces an ordered layer at the interface. This order is transmitted to the

bulk liquid crystal by elastic forces and it changes the behavior of nematogens, e.g., by shifting the transition temperature and changing the order of the transition at a critical thickness. The existence of such a critical thickness arises from the existence of an ordering field exerted by the walls. This field may be compared to an external magnetic field capable of aligning the molecules with itself (see Ref. [19] and references therein). In the present study we show that, similar to the effect of an external field [12], confinement promotes the Saturn ring configuration. More specifically, our results indicate that confined micrometer particles may be surrounded by a stable Saturn ring disclination line. These results are in distinct contrast with the situation in the bulk, and help explain recent observations of Saturn ring defects surrounding micrometer-sized particles confined between two walls [20].

The paper is organized as follows. In Sec. II, we introduce the elastic free energy for the nematic liquid crystal and describe in detail the numerical procedure employed for its minimization. For the complex geometry of interest to this work, the minimization of the free energy is performed using finite elements. In Sec. III, we present and discuss our results.

II. MINIMIZATION OF THE FRANK ELASTIC FREE ENERGY

A. The elastic free energy

In an ideal nematic liquid crystal, the common, average direction of the molecules is characterized by the director $\pm\mathbf{n}(\mathbf{r})$. The insertion of a spherical particle in the nematic liquid crystal as well as the constraints imposed by the orientation of the liquid crystal at a surface distorts the uniform alignment. The free energy of slowly varying spatial distortions is determined by the Frank free energy [21]

$$F_e = \int d^3\mathbf{r} f_e(\mathbf{r}) + \int dS f_s(\mathbf{r}), \tag{1}$$

where f_e is the elastic free energy density,

$$f_e = \frac{1}{2}\{K_1(\boldsymbol{\nabla}\cdot\mathbf{n})^2 + K_2(\mathbf{n}\cdot\boldsymbol{\nabla}\times\mathbf{n})^2 + K_3[\mathbf{n}\times(\boldsymbol{\nabla}\times\mathbf{n})]^2\}, \tag{2}$$

and f_s is the surface free energy density

$$f_s = \frac{1}{2} W[1-(\mathbf{n}\cdot\hat{\boldsymbol{\nu}})^2]. \tag{3}$$

The free energy density f_e describes the distortions in the director field $\mathbf{n}(\mathbf{r})$. The elastic constants K_1, K_2, and K_3 correspond to the splay, twist, and bend deformations, respectively. The surface free energy density f_s (or Rapini-Papoular term [22]) takes into account the contribution from the surfaces, and the vector $\hat{\boldsymbol{\nu}}$ indicates the preferred orientation at the surfaces. As discussed in the literature for particle in the bulk [10,13], the director structure depends on the effect of the relative strength of the nematic bulk elasticity and the director anchoring. When the anchoring is weak, the director field perturbations are small and present quadrupolar symmetry. On the other hand, for strong homeotropic anchoring, both hedgehog defects and Saturn rings are possible. In close analogy to the experimental realization, where topological defects have been observed around solid particles in a confined geometry [20], in the present work we consider the case of strong homeotropic anchoring at the surface of the particle, and also strong planar anchoring at the walls. (In the experimental realization, the strength of the anchoring is controlled by self-assembled monolayers of $CH_3(CH_2)_9SH$ and $CH_3(CH_2)_{15}SH$ of different composition [20]). For these strong anchoring conditions, the director $\mathbf{n}$ is aligned with the preferred direction $\hat{\boldsymbol{\nu}}$, and the surface free energy f_s is equal to zero.

When defects are present in the system, the elastic Frank free energy becomes singular at the core defect. As it is well known, a treatment in terms of the director is not appropriate to describe the structure of the core defects. To investigate in detail the core defect, one should work with the traceless symmetric tensor order parameter $\mathbf{Q}_{\alpha\beta}$. More specifically, as it is has been shown [23], the structure of the core defect is characterized by strong biaxiality and a strong decrease in the nematic order parameter which reflects that the liquid crystal ''melts'' locally at the point defect. In the following section, we explain how the contribution to the free energy coming from the neighborhood of the core defect is approximately taken into account.

The equilibrium configuration of the director $\mathbf{n}(\mathbf{r})$ is obtained by minimization of the Frank free energy, Eq. (1). The minimization of the free energy requires solution of a nonlinear Euler-Lagrange equation. One possible method is to use a finite representation of the derivatives to solve the Euler-Lagrange equation [12]. Since the geometry considered in this work is nontrivial, we prefer to use the method of finite elements [24].

B. The geometry and the numerical procedure

The geometry of the system is presented in Fig. 1. A spherical particle of radius R is confined to a cylinder of radius R_c and length L_z. The particle is located on the axis of the cylinder and the system exhibits axial symmetry. We use cylindrical coordinates and assume that the director is located in the plane (ρ,z) and is characterized by the tilt angle $\theta(\rho,z)$,

$$\mathbf{n}(\rho,z) = \sin\theta(\rho,z)\mathbf{e}_\rho + \cos\theta(\rho,z)\mathbf{e}_z, \tag{4}$$

where $(\mathbf{e}_\rho,\mathbf{e}_z)$ is the local coordinate basis. The constraint imposed on the director to be in the plane (ρ,z) implies that the twist term in the free energy [Eq. (2)] is zero, and that the model does not allow for possible twist transitions (as it may happen for the hedgehog defect [12]). To allow for a twist transition, one has to take into account the ϕ degeneracy on the director. As we show in the following section, the quantitative changes in the free energy when one does not introduce this additional degree of freedom are so small that this approximation is of little consequence to the present study.

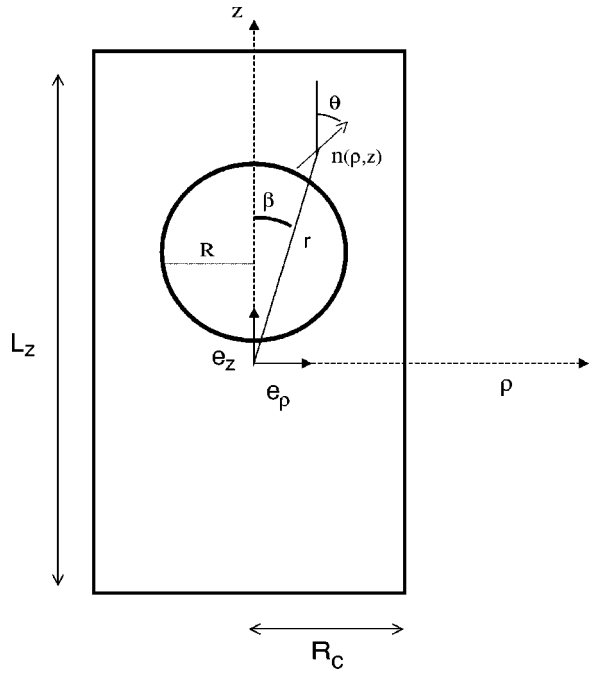

FIG. 1. Geometry of the system. The origin of the coordinate system is located in the middle of the cylinder. R is the radius of the particle, R_c the radius of the cylinder, and L_z its length. The director $\mathbf{n}(\rho,z)$ is defined by the tilt angle $\theta(\rho,z)$.

Under the assumption of Eq. (4), we write the Frank free energy density in units of K_3/R^2,

$$\tilde{f}_e(\theta)=\frac{f_e}{K_3/R^2}=\frac{\tilde{K}_1}{2}\left(\frac{\sin\theta}{\rho}+\frac{\partial\theta}{\partial\rho}\cos\theta-\frac{\partial\theta}{\partial z}\sin\theta\right)^2+\frac{1}{2}\left(\frac{\partial\theta}{\partial z}\cos\theta+\frac{\partial\theta}{\partial\rho}\sin\theta\right)^2, \tag{5}$$

where $\tilde{K}_1=K_1/K_3$ and all lengths are now given relative to the radius R of the spherical particle. The ratio $\tilde{K}_1$ of the elastic constants is fixed at $\tilde{K}_1=0.79$, which is representative of a pentylcyanobiphenyl (5CB) liquid crystal at room temperature [2].

For symmetry reasons, the minimization of the reduced free energy

$$\tilde{F}_e=\int d^3\mathbf{r}\tilde{f}_e(\theta) \tag{6}$$

is performed in the restricted two-dimensional region defined by $-L_z\leqslant z\leqslant L_z$ and $0\leqslant\rho\leqslant R_c$. The area of integration is covered by a net of triangles. This net is generated with FLUENT software that permits the size of the triangles (or the characteristic mesh resolution b) to be specified with arbitrary precision. The calculations presented here are performed with a mesh division of $b=0.05$ or $b=0.025$ (in units of R). This precision offers a good description of the director distribution in the neighborhood of defects, where it varies rapidly on short length scales. Furthermore, it allows us to determine the precise location of the defects. Each triangle defines an element and is characterized by its three vertices. The number of elements depends on the size of the cylinder and on the mesh division. For a cylinder with $R_c=3$ and $L_z=4$, the number of elements is of order $N\approx 9000$ and $N\approx 37\,000$, for $b=0.05$ and $b=0.025$, respectively.

The director field $\mathbf{n}(\mathbf{r})$ is now described by a set of N vectors, where N is the number of vertices i. At each vertex, the director is characterized by the tilt angle θ_i. Due to the symmetry $\mathbf{n}\rightarrow-\mathbf{n}$, the angle θ_i is restricted to lie in the range $[0,\pi]$. The functional minimization of the free energy, $\delta\tilde{F}_e/\delta\theta(\mathbf{r})=0$, is transformed into the minimization of the function $\tilde{F}_e(\{\theta_i\})$ with respect to the N variables $\{\theta_i\}$. With finite elements, the minimization of the free energy is performed directly, without need for the Euler-Lagrange equations. The principles of the numerical procedure are the same as those used in Ref. [24]. The free energy is written as the sum

$$\tilde{F}_e(\{\theta_i\})=\sum_{j=1}^{N_t}\tilde{F}_e^j(\theta_1^j,\theta_2^j,\theta_3^j), \tag{7}$$

where the index j runs over all the N_t triangles of the mesh. $\tilde{F}_e^j(\theta_1^j,\theta_2^j,\theta_3^j)$ is the free energy of the triangle j, and the angles $(\theta_1^j,\theta_2^j,\theta_3^j)$ are the tilt angles of the director at the corresponding three vertices. To evaluate the free energy for each triangle of area $\mathcal{A}_j$, namely,

$$\tilde{F}_e^j=2\pi\int_{\mathcal{A}_j}dz\,d\rho\,\rho\tilde{f}_e(\theta[\rho,z]), \tag{8}$$

it is convenient to introduce the coordinates v and w defined by

$$\rho^j(v,w)=\rho_1^j+(\rho_2^j-\rho_1^j)v+(\rho_3^j-\rho_1^j)w, \tag{9}$$

$$z^j(v,w)=z_1^j+(z_2^j-z_1^j)v+(z_3^j-z_1^j)w. \tag{10}$$

Here (ρ_i^j,z_i^j) are the coordinates of the vertices attached to the triangle j. The free energy of the triangle j [Eq. (8)] is then given by the integral

$$\tilde{F}_e^j=2\pi\Delta_j\int_0^1 dw\int_0^{1-w}dv\,\rho^j(v,w)\tilde{f}_e(\theta[v,w]), \tag{11}$$

where Δ_j is the Jacobian determinant of the coordinate transformation, Eqs. (9) and (10). To evaluate the integral, Eq. (11), one assumes that the distribution of the tilt angle $\theta(v,w)$ inside the small element is given by a linear interpolation,

$$\theta^j(v,w)=\theta_1^j+(\theta_2^j-\theta_1^j)v+(\theta_3^j-\theta_1^j)w, \tag{12}$$

and that ρ is given by the average value $\rho^j=(\rho_1^j+\rho_2^j+\rho_3^j)/3$. The partial derivatives of $\theta(\rho,z)$, which are required for the evaluation of the Frank free energy are derived from the distribution, Eq. (12), and from the coordinate transformation, Eqs. (9) and (10). In this framework, one is

able to evaluate the free energy over the entire area of integration for any given distribution of the angles $\{\theta_j\}$.

In the numerical procedure, an initial configuration is introduced, which describes approximately the director distribution for a given defect. To minimize the free energy, we relax the configuration towards equilibrium using a Newton-Gauss-Seidel method [25],

$$\theta_i^{new} = \theta_i^{old} - \left[\left(\frac{\partial \tilde{F}_e}{\partial \theta_i} \right) \Big/ \left(\frac{\partial^2 \tilde{F}_e}{\partial \theta_i^2} \right) \right]. \tag{13}$$

The derivatives of the free energy with respect to θ_i are evaluated numerically. Once a new tilt angle θ_i^{new} is computed, it is systematically inserted in the configuration for the evaluation of the next tilt angle. Note that the location of the defect is fixed in the initial configuration, and it is observed not to move during the relaxation procedure (for both the Saturn ring defect as well as the hedgehog defect). Similar phenomena have been observed in other works [12,24], indicating that the numerical procedure does not allow the point defect to move automatically into its local minimum. To find the local minimum, one has thus to plot the free energy as a function of the location of the defect.

III. RESULTS

The orientation of the liquid crystal at the surfaces of the cylinder is described in what follows. We assume strong planar anchoring at the surface $\rho = R_c$, and strong homeotropic anchoring at the walls $z = \pm L_z/2$. With these anchoring conditions, the average orientation of the liquid crystal at a large distance from the particle is in the $\mathbf{e}_z$ direction. At the surface of the particle, we specify strong homeotropic anchoring conditions. For these anchoring conditions, the particle may be accompanied by two defects: the Saturn ring disclination line or the hedgehog point defect. In this section, we present and discuss the results for these two defects.

A. Saturn ring disclination line

As an initial configuration, we use an expression coming from the ansatz function introduced in Ref. [10]. For a particle located at the origin of the coordinate system, an approximate expression of the Saturn ring configuration is given by the tilt angle

$$\theta(r,\beta) = \beta - \frac{1}{2}\arctan\left(\frac{\sin 2\beta}{1/f(r) + \cos 2\beta} \right), \tag{14}$$

where $f(r)$ is a unique function of r and (r,β) are the spherical coordinates (see Fig. 1). This function must satisfy some constraints to be compatible with the anchoring conditions at the different surfaces of the system. The explicit form of $f(r)$ for a particle in a bulk nematic is given in Ref. [10]. Here, we use expression (14), with

$$f(r) = (a/r)^3, \tag{15}$$

for a distance r smaller than a fixed value a, and the corresponding asymptotic form

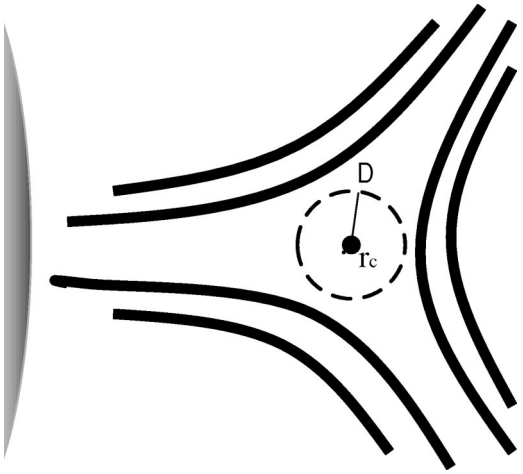

FIG. 2. Particle surrounded by a disclination line. A small cylinder of radius D is cut around the core defect of radius r_c.

$$\theta(r,\beta) = a^3 \frac{\sin 2\beta}{r^3}, \tag{16}$$

for a distance r greater than this value a. With this initial configuration, the Saturn ring defect is located at $\rho = a$ and $z = 0$ [since $\theta(z=0,\rho \to a^-) \to \pi/2$ and $\theta(z=0,\rho \to a^+) \to 0$]. In the neighborhood of the surface of the particle, the constraint $f(r=R)=1$ compatible with the homeotropic anchoring is not satisfied. However, this has no consequences since the strong homeotropic anchoring at the surface of the particle is imposed in the numerical procedure, and the director field goes to the equilibrium configuration compatible with this anchoring condition.

We let the system relax to its equilibrium configuration and compute the resulting elastic free energy $\tilde{F}_e$. This procedure assigns a free energy to the disclination line, which is certainly not correct. As mentionned previously, to investigate in detail the core structure, one should work with the traceless symmetric tensor order parameter $Q_{\alpha\beta}$ [26]. In the neighborhood of the defect, we thus expect that the numerical estimates given by the continuum theory are not reliable below a certain length scale. To obtain an estimate on the total free energy in the neighborhood of the defect, we cut a small cylinder of radius D surrounding the core defect (see Fig. 2). The position of the core defect is determined automatically by looking for the local maximum in the elastic free energy. The location of this maximum defines the center of the cut cylinder. The total free energy of the system $\tilde{F}$ is then given by

$$\tilde{F} = \tilde{F}_e + \tilde{F}_D, \tag{17}$$

where $\tilde{F}_e$ is now the elastic contribution over the entire area of integration without the cut cylinder and $\tilde{F}_D$ is the free energy of the small cylinder. (In the remainder of this work, all numerical estimates of the total free energy F are given in reduced units $\tilde{F} = FR^2/K_3$.) The evaluation of $\tilde{F}_D$ should include a contribution coming from the free energy of the

core defect and also an elastic contribution coming from the region that extends outside the core radius r_c (see Fig. 2). Here, we estimate the free energy density $\tilde{f}_D$ per unit length ($\tilde{F}_D = 2\pi a \tilde{f}_D$) using the approximate expression

$$\tilde{f}_D = \frac{\pi}{4}\left[\frac{1}{2} + \ln\frac{D}{r_c}\right]. \tag{18}$$

The first term in the expression, Eq. (18), corresponds to the free energy of the core defect of radius r_c and the second term is the elastic free energy around the core defect of the half-integer disclination line. Both expressions are obtained in the one-constant approximation [27]. One could improve quantitatively the estimate of $\tilde{f}_D$, but this should not have any significant consequence on the present study. To be consistent, the evaluation of the total free energy should not depend on the radius D of the cut cylinder. We have checked the convergence of total free energy as the radius D is increased using different values of the mesh of the grid ($b = 0.05$ and $b = 0.025$) and changing the area πD^2 of the cut cylinder. For instance, fixing the radius of the Saturn ring at $a = 1.25R$ and taking $r_c = 0.005$, we have evaluated the total free energy for four sizes of the cut cylinder, with D varying from $D = 0.01$ to $D = 0.05$. The estimates on the total free energy converge to a common value ($\tilde{F} \approx 37.5$) within the accuracy of order $\Delta\tilde{F}/\tilde{F} \approx 1\%$. These small numerical variations allow for a good estimate of the total free energy and, as we will see below, are very small compared to the changes in the free energy induced by the confinement.

The core defect is located in the middle of the cut cylinder (see Fig. 2), but its radius is not known *a priori*. Following the analysis presented by Stark [12], we use this property to introduce an absolute length into the geometry of the system. The radius of the core defect is considered as a parameter, and D gives an upper bound for r_c. (For instance, the value of r_c is taken to be $r_c = 0.005$ or $r_c = 0.05$ in units of R). An absolute length scale is introduced by fixing r_c to its characteristic size, which is of order 10 nm [27] ($r_c = 0.005$ corresponds to a sphere of radius $R = 2\ \mu$m).

The structure of the director field for a particle surrounded by a Saturn ring defect is represented in Fig. 3. In this figure, the ring is located at a distance $a = 1.25R$. The radius of the cylinder is $R_c = 3$, and its length is $L_z = 4$. In this optical picture, we have represented the director profile when the light is transmitted through two crossed polarizers in the $\mathbf{e}_\rho$ and $\mathbf{e}_z$ directions. (The bright area corresponds to $\theta = \pi/4$ when the light is transmitted and the dark area corresponds to $\theta = 0$ or $\theta = \pi/2$ when the director is aligned in the direction of one of the polarizers.)

B. Hyperbolic hedgehog point defect

For a particle surrounded by the hedgehog point defect, we use as the initial configuration the ansatz function obtained from the study of structure of the defect in the bulk [3]. When the particle is located in the middle of the cylinder, the director is approximately described by the tilt angle

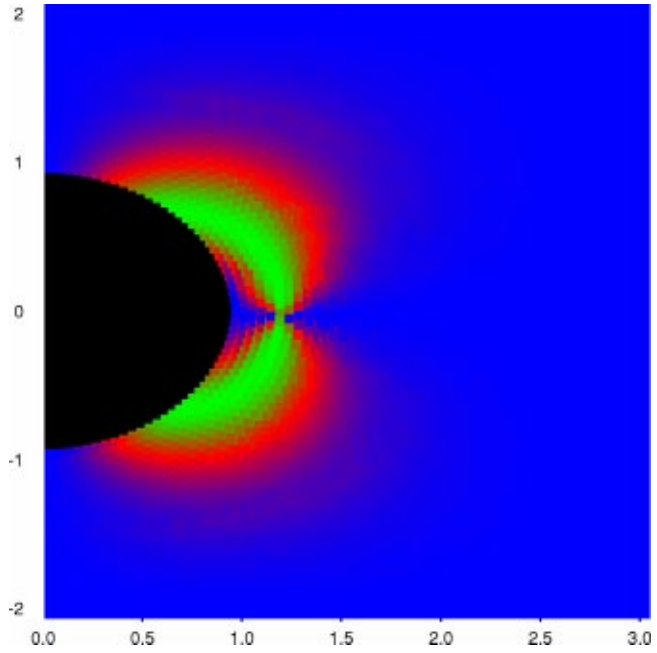

FIG. 3. (Color online only) Director configuration for a particle surrounded by the Saturn ring disclination line. In this optical picture, the dark area corresponds to $\theta = \pi/2$ or $\theta = 0$, and the bright area corresponds to $\theta = \pi/4$.

$$\theta(r,\beta) = 2\beta - \arctan\left(\frac{r\sin\beta}{r\cos\beta + a}\right) - \arctan\left(\frac{ar\sin\beta}{ar\cos\beta + 1}\right) + h(a,r,\beta), \tag{19}$$

where a is the distance between the particle and the defect, and the function $h(a,r,\beta)$ is introduced to ensure the correct far-field behavior [the explicit form of $h(a,r,\beta)$ is given in Ref. [3]].

The extension of the point defect is also of order 10 nm. In that case, the treatment of the hedgehog point defect is more straightforward than that of the Saturn ring disclination line; the contribution in the total free energy coming from the defect is small and induces changes less than $\Delta F/F = 1\%$. This difference between the two configurations comes from the fact that the hedgehog defect is a point defect. The free energy associated with the point defect is of order $K_3 \times 10$ nm. As long as one is concerned with particles of radius greater than 100 nm, this quantity represents less than 1% of the total free energy and can be neglected [12]. As mentioned previously, the absolute length of the system is introduced by fixing the radius r_c of the core defect to a certain value. For a given geometry, when the particle is surrounded by a Saturn ring defect, the total free energy $\tilde{F}$ of the system varies as r_c is changed. This variation is associated with the varying length of the disclination line. On the other hand, when the particle is surrounded by the hedgehog point defect, the total free energy of the system stays constant and does not depend on r_c. Indeed, since the free energy associated to the point defect is not taken into account, the total free energy of the system is given by the elastic Frank free energy which is constant when all lengths are

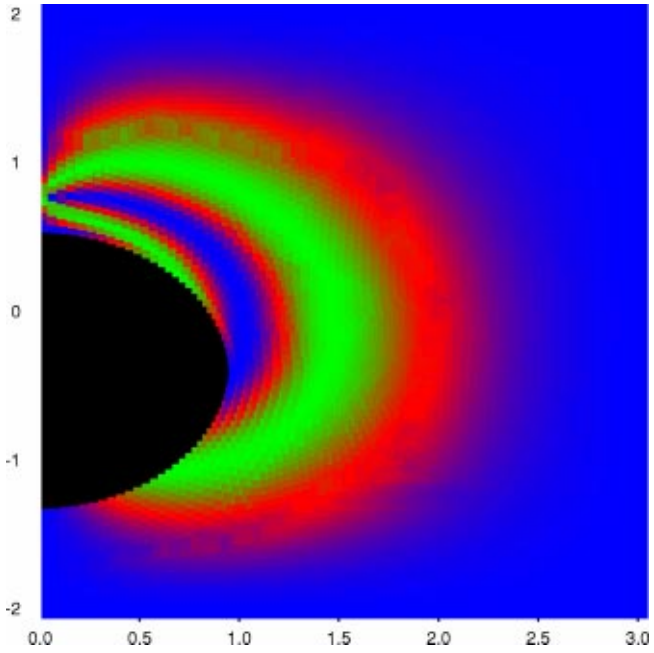

FIG. 4. (Color online only) Director configuration for a particle surrounded by a hedgehog point defect. The particle is located at its equilibrium position $z \approx -0.4$ (see the discussion in the text). The color key is the same as in Fig. 3.

expressed in units of R. The reduced free energy $\tilde{F}$ is thus independent on the size of the particle. (This approximation should be reasonable as long as the particle is bigger than $R \approx 100$ nm and that the contribution from the core defect can be neglected.)

The structure of the director field for a particle surrounded by a hedgehog defect is represented in Fig. 4. The point defect is located at a distance $a=1.2R$, the radius of the cylinder is $R_c=3$, and its length is $L_z=4$.

C. Discussion

We have determined the size of the cylinder, which corresponds to the bulk conditions for the two defects. We assume that the bulk limit is recovered once the elastic free energy remains constant as the size of the cylinder is increased in one of the two directions, $\mathbf{e}_\rho$ and $\mathbf{e}_z$. This analysis provides an estimate of the lengths beyond which the defect does not distort the uniform alignment of the nematic liquid crystal.

We consider first a cylinder with $R_c=3$ and $L_z=4$. The particle is fixed on the axis of the cylinder and is progressively moved axially from the center $z=0$ to one of the surfaces. The variation between positions is $\Delta z=0.2$. To evaluate the ensuing changes in the elastic free energy, the parameter b has to be small compared to Δz. Here, the mesh is fixed at $b=0.005$. The variations in the free energy, $\tilde{F}(z)-\tilde{F}(z=0)$, are reported in Fig. 5. For a particle surrounded by a Saturn ring, the free energy remains unaltered for a small displacement of the particle from the center: the free energy for $z=0$ is the same as for $z=-0.2$ (within numerical accuracy). This indicates that $L_z=4$ corresponds

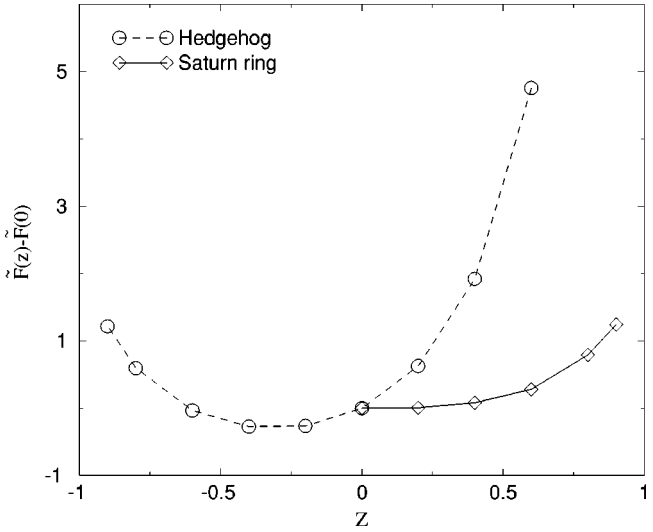

FIG. 5. Variation of the elastic free energy, $\tilde{F}(z)-\tilde{F}(0)$, as the particle is moved away from the center of the cylinder ($R_c=3, L_z=4$). A particle surrounded by a hedgehog defect is trapped by the elastic forces at the position $z \approx -0.4$.

to the bulk limit. [The Saturn ring is located here at $a=1.25R$; and for a 2-μm particle, $\tilde{F}(0) \approx 37.50$]. As the particle gets closer to the horizontal surface, the surface creates a repulsive force corresponding to the distortion of the director induced by the spherical shape of the particle and the plane geometry of the surface. Due to the symmetry of the Saturn ring configuration, the particle is trapped between the two horizontal surfaces. If the size of the cylinder is increased in the ρ direction to $R_c=4$, the free energy does not change (the variation of the free energy as R_c is decreased is discussed in the next paragraph, and the data for $R_c=3$ and $R_c=4$ are reported in Fig. 8). Thus, when the particle is surrounded by the Saturn ring, the bulk limit is recovered when $R_c=3$ and $L_z=4$. In contrast, when the particle is accompanied by a hedgehog defect, a small displacement of the particle from the center induces a change in the free energy (see Fig. 5). [The hedgehog defect is here located at $a=1.2R$ and $\tilde{F}(0) \approx 23.97$.] This result indicates that the particle interacts with the confining horizontal surfaces through elastic forces even at $z=0$. The energetic contribution arising from the distortion as the point defect approaches the surface is large, and is indicative of a considerable repulsive force between the wall and the point defect. A particle accompanied by the hedgehog defect in a confined geometry is thus trapped by elastic forces at a nonsymmetric location to balance these two repulsive forces of different magnitudes. When $R_c=3$ and $L_z=4$, the equilibrium location of the particle is at $z \approx -0.4$. For the hedgehog configuration, one has to increase the size of the cylinder in the two directions to recover the bulk limit. We find that the bulk limit is recovered when $R_c=4$ and $L_z=6$.

We have studied the evolution of the total free energy as the positions of the point defect and of the ring are changed. The results are reported in Fig. 6 in the bulk limit for a particle with $R=2$ μm. To obtain the location of the defect with useful accuracy, the mesh of the grid is fixed here at the

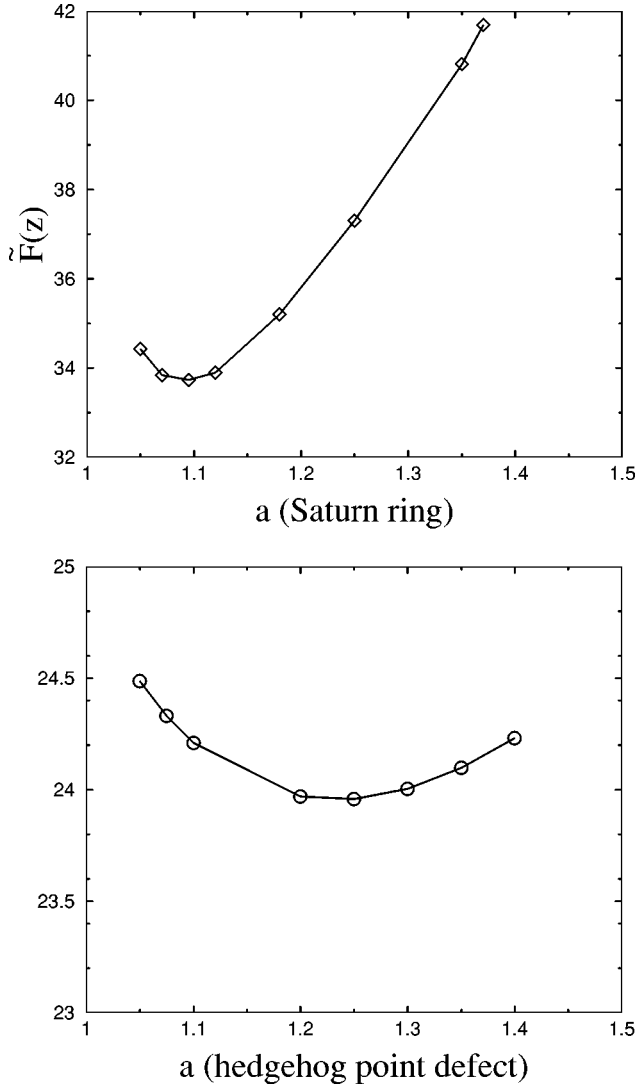

FIG. 6. Total free energy for various locations of the Saturn ring disclination line (top) and the hedgehog point defect (bottom), in the bulk limit and for $R=2$ μm.

value $b=0.025$. The equilibrium position of the ring is $a \approx 1.10R$. This estimate is consistent with previous estimates obtained with ansatz functions $a \approx 1.25R$ [10] and $a \approx 1.08R$ [3]. It is also closed to the results obtained with Monte Carlo simulation [13]. This method predicts $a \approx 1.13R$ in the limit of strong homeotropic anchoring on sphere surface. It is in very good agreement with the value $a=1.10R$ obtained by numerical minimization [12] (in the one-constant approximation and for $R=0.72$ μm), and it agrees with experimental values $a=(1.091\pm 0.005)R$ and $a=(1.095\pm 0.003)R$ [20] (these values were measured for particles with $R=100$ μm and $R=60$ μm, respectively). For the hedgehog configuration, the distance from the particle to the point defect is between $a=1.20R$ and $a=1.25R$. This estimate of the position of the point defect is in good agreement with the estimate $a=1.17R$, obtained with a trial function [1], and with the value $a=(1.26 \pm 0.02)R$ obtained by numerical minimization [12]. It is closed to the Monte Carlo results [13] in the strong anchoring limit $a \approx 1.22R$. We observe that the minimum in free energy is lower for the hedgehog configuration than for the Saturn ring configuration. This result suggests that in the bulk, a particle with $R=2$ μm is accompanied by a stable hedgehog defect. This analysis has already been performed by Stark [12] to interpret the experimentally observed defects that arise with micrometer-sized particles. We have verified the accuracy of our calculations and compared our results to those of Stark; the results for the total free energy for various sizes of particle are reported in Fig. 7. The agreement is quantitative (to make the comparison between $\overline{F}$ in Ref. [12] and $\tilde{F}$, one has to take into account the factor π). Our results indicate that for a particle in the bulk and smaller than $R=250$ nm, the Saturn ring configuration is more stable than the hedgehog, which is in very good agreement with the past analysis [12].

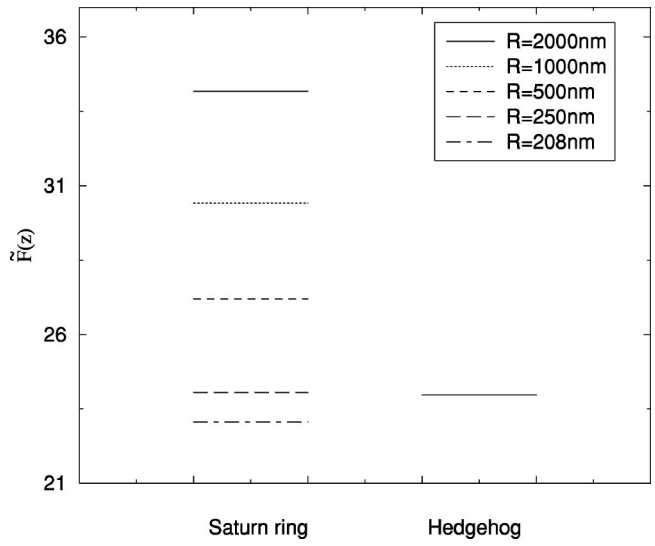

FIG. 7. Transition from Saturn ring to hedgehog defect for a particle in the bulk.

The effects of confinement are investigated first by decreasing the radius of the cylinder. For each defect, the length L_z is fixed at the value corresponding to the bulk limit in the z direction. In Fig. 8, we have reported the total free energy of the system for a particle with $R=2$ μm, in both the Saturn ring and hedgehog defect cases. Five geometries have been considered, namely $R_c=4,3,1.4,1.3$, and $R_c=1.2$. We find that the radius of the ring defect decreases as the radius of the cylinder decreases. For a very small cylinder, we note indeed a significant shift in the equilibrium position of the defect when compared to the equilibrium location in the bulk limit: the radius of the ring is approximately located at $a \approx 1.08R$ when $R_c=1.2$, in contrast to $a \approx 1.10R$ when $R_c=4$. This shift corresponds to the elastic force exerted by the walls, which tends to align the molecules in the z direction and pushes the defect closer to the particle. The location of the hedgehog defect is also slightly shifted under the effect of confinement. We find that the defect is located at $a \approx 1.20R$ for $R_c=1.2$. The total free energy reported in Fig. 8 corresponds to $a=1.20R$ (on this scale, one cannot distinguish the difference in the total free energy between a

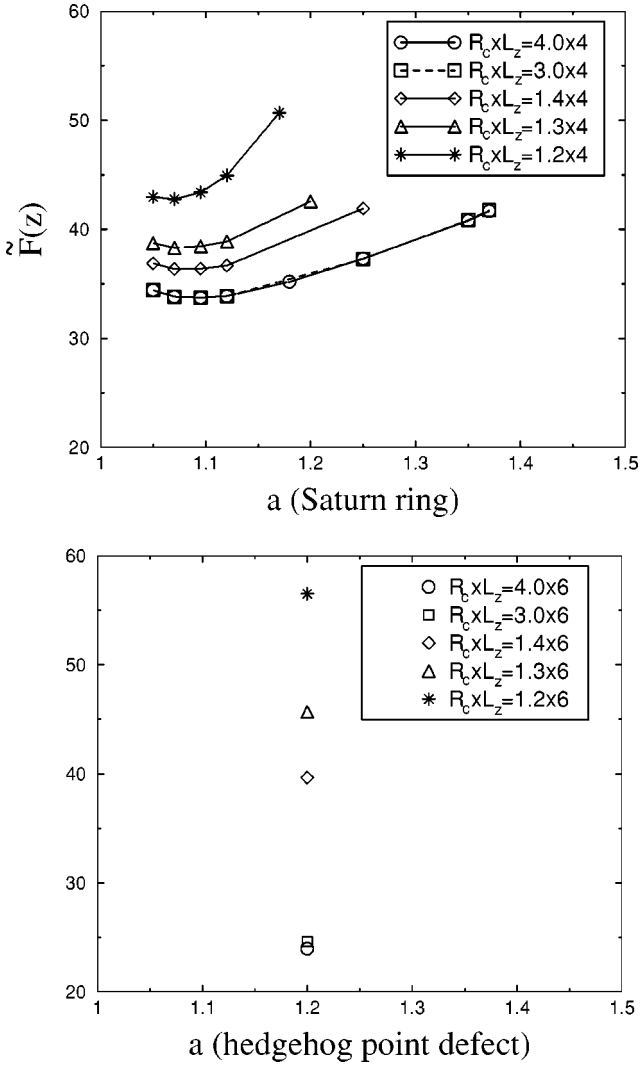

FIG. 8. Total free energy for a particle with $R=2$ μm, surrounded by a Saturn ring (top) and by a hedgehog defect (bottom), for various radii R_c of the cylinder.

$=1.20R$ and $a=1.25R$). The results serve also to emphasize that the distortion of the director created by the confining surfaces induces a strong increase in the elastic free energy. For example, for a particle with $R=2$ μm confined to a small cylinder of radius $R_c=1.2$, confinement leads to a reversal of stability in which the Saturn ring configuration becomes more stable than the hedgehog configuration. Thus, in contrast to the bulk situation, the Saturn ring configuration is expected to be more stable than the hedgehog defect for a micrometer particle. We have performed this analysis for three different particle sizes ($R=2$ μm, $R=40$ μm, and $R=100$ μm). The results are reported in Fig. 9 for a particle confined to a cylinder of radius $R_c=1.2R$. For this geometry, our results indicate that the transition from the Saturn ring to the hedgehog defect occurs at a radius of $R=20$ μm. The net effect of the neighboring surfaces is thus to promote the stability of the Saturn ring.

These results on the effect of confinement should be compared qualitatively with the effect of external magnetic (or electric) fields. The study reported by Stark [12] indicates

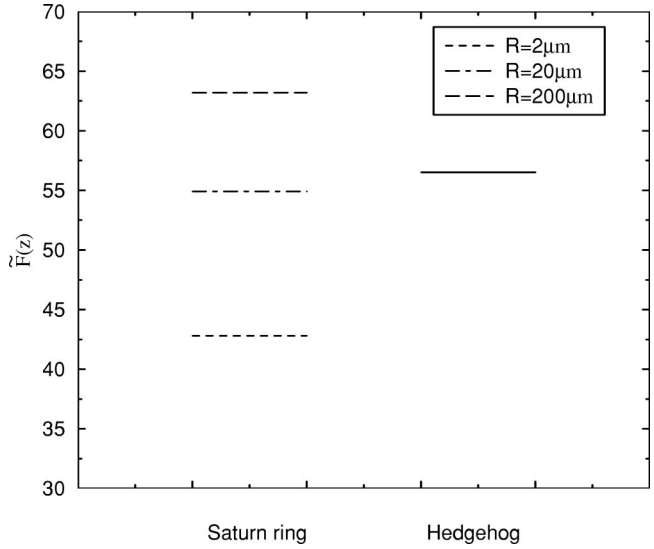

FIG. 9. Transition from Saturn ring to hedgehog defect for a particle confined by a cylinder with $R_c=1.2R$.

that the stability of the Saturn ring configuration, for a particle in the bulk, is promoted by an external field applied in the direction of the symmetry axis (the z direction). For positive anisotropic susceptibility (or permittivity), the applied magnetic field tends to align the molecules in the direction of the external field. In the present study, liquid crystals at all various confining surfaces are aligned in the z direction. The order at the surfaces is transmitted to the bulk through elastic forces, and the wall acts as an external field (promoting the Saturn ring configuration).

In a recent experiment [20], Gu and Abbott have observed particles of radii ranging from $R=40$ μm to 100 μm, surrounded by a Saturn ring. The particles are immersed in nematic 5CB and confined between two walls separated by a distance of 120 μm (and with the same anchoring conditions as in the present study). Some of these Saturn ring defects were observed to be stable for over 1 month. Spontaneous transformations of Saturn ring defects to other types of defects were also observed. The transformed configurations have a dipolar symmetry, like the symmetry of the hedgehog defect, but cannot be definitively classified as hedgehog point defects. These experiments indicate also that the Saturn ring is not exactly located in the equatorial plane of the particle but it deviates from it, exhibiting some oscillations. The deformation of the Saturn ring may be an effect induced by the presence of the two confining walls. Indeed, the two vertical walls should affect the axial symmetry of the Saturn ring configuration and thus distort slightly the disclination line. The existence of these Saturn rings for durations of over 1 month, and the fact that they form for such large particles (40 μm$\leqslant R\leqslant 100$ μm) suggest that the confinement induced by the walls influences the metastability of the Saturn ring and pathways that convert Saturn rings to point defects.

To establish a comparison between these experiments and the present work, some precautions must be taken. First, the geometry of the present system differs from the experiments; the results presented here concern particles in a cylinder. Second, the present study addresses the effect of confinement

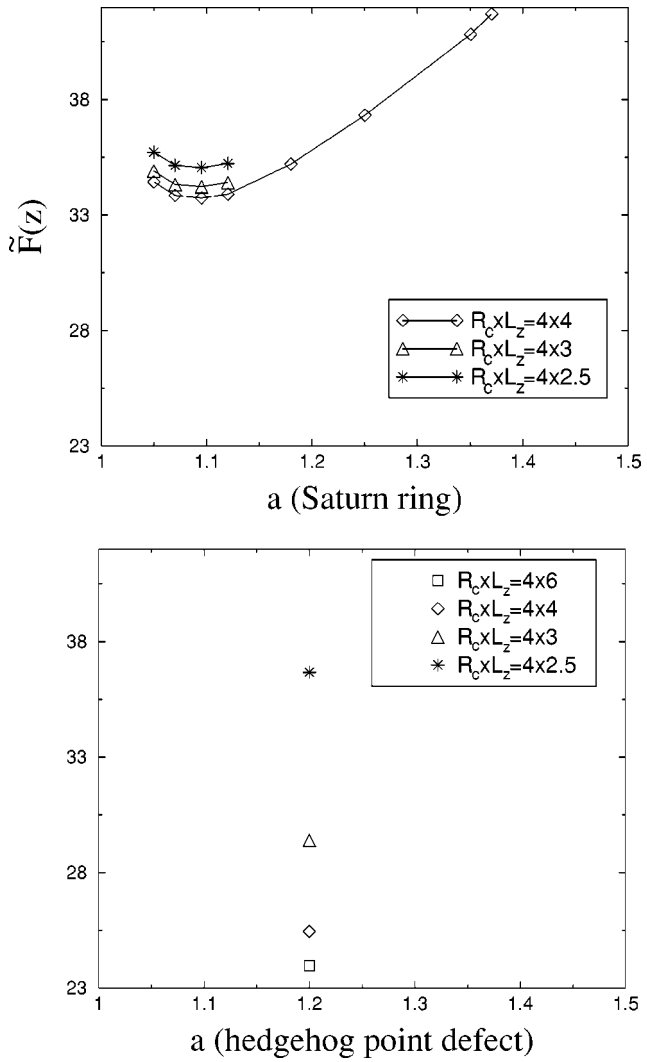

FIG. 10. Total free energy for a particle with $R=2$ μm, surrounded by a Saturn ring (top) and by a hedgehog defect (bottom), confined between two horizontal plates with various lengths L_z of the cylinder.

on the stability of the defects and does not give any information on metastability or pathways that convert a Saturn ring to other defects. Qualitatively, this study indicates that the Saturn ring configuration is promoted by confinement and that it can become the most stable configuration in a confined geometry. For instance, a particle with $R=2$ μm should be surrounded by a stable Saturn ring when confined in a cylinder with $R_c/R=1.2$. On the other hand, as Fig. 9 indicates, for the same value of the ratio $R_c/R=1.2$, the Saturn ring configuration for particles of radii $R=40$ μm and $R=100$ μm is not the most stable one, compared to the hedgehog. (In experiments, spontaneous, transformed configurations are observed in a slightly different geometry, with particles of radii $R=40$ μm and $R=100$ μm, and with a separation of 120 μm between the two vertical walls.) From the experiments and from the present study, one can thus conclude that confinement influences both the metastability and the stability of the Saturn ring configuration.

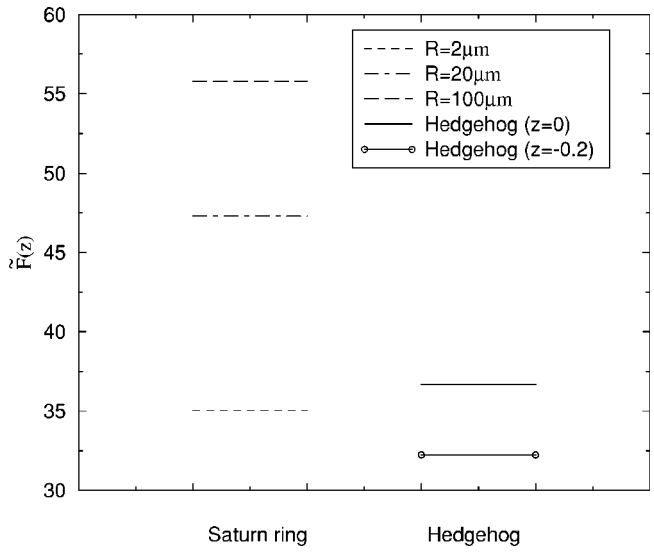

FIG. 11. Transition from Saturn ring to hedgehog defect for a particle confined between two horizontal plates with $L_z=2.5R$.

We have performed the same analysis by confining the particle between two plates. This is achieved by decreasing the length L_z of the cylinder and fixing the radius R_c to the bulk value. In this geometry, the confining surfaces are thus parallel to the plane defined by the Saturn ring disclination line. The total free energy for the values $L_z=4,3,2.5$ is reported in Fig. 10, for both the Saturn ring and the hedgehog defects. For the hedgehog defect we have also reported on the total free energy in the bulk limit $L_z=6$. In this figure, the radius of the particle is fixed at $R=2$ μm, and the particle is located in the middle of the layer. The transition from the Saturn ring to the hedgehog is summarized in Fig. 11, for $L_z=2.5$. For this geometry, as mentioned previously, the equilibrium location of a particle surrounded by the hedgehog defect is not in the middle of the two plates, but the particle is trapped at a shifted vertical position. In Fig. 11, we have reported the free energy when the particle is in the middle of the layer and when the particle is trapped at its shifted equilibrium position near one of the surfaces. According to these results, for $R=2$ μm, a particle near the surface, which is accompanied by the hedgehog defect is more stable than a particle in the middle, which is accompanied by the Saturn ring. Thus, for a distance $L_z=2.5$, the transition between the two defects occurs slightly below $R=2$ μm. From these results, we conclude that the confinement between two horizontal plates is qualitatively similar to the confinement in a small cylinder, promoting also the Saturn ring configuration. In the cylinder $R_c/R=1.2$, the transition occurs around $R=20$ μm, whereas for the present geometry with $L_z=2.5$, the effect of confinement is less pronounced with a transition occurring around $R=2$ μm. These predictions also appear relevant to the past experimental observations. Past experiments conducted with particles of radii ranging from 40 μm to 100 μm and confined between two horizontal walls with homeotropic anchoring separated by 120 μm indicate that the Saturn ring is not long lived. These observations suggest that the effect of confinement is less pronounced in this geometry than when the particle is confined

between two vertical walls with planar anchoring. It would be interesting to conduct additional experiments with this geometry and using micrometer-sized particles, to investigate the possible coexistence of the two defects with the shifted equilibrium position of the particle accompanied by a hedgehog defect.

IV. CONCLUSION

In this paper, we have determined the structure of the director field around a particle immersed in a confined nematic liquid crystal. We have considered strong homeotropic anchoring conditions at the surface of the particle and studied the transition from the Saturn ring to the hedgehog defect. The results obtained in the bulk limit agree well with previous analyses. In particular, for a particle in the bulk, we find that the hedgehog configuration is more stable than the Saturn ring when the radius of the particle is larger than $R = 250$ nm. We have investigated the effect of confining surfaces on the transition between the two configurations by considering a particle confined in a cylinder and between two plates. For a particle of radius $R = 2$ μm and confined by a cylinder of radius $R_c = 1.2R$, we have shown that the confining surfaces cause a reversal of the stability, in which the Saturn ring configuration becomes more stable than the hedgehog configuration. These results contrast with the bulk and indicate that, for both geometries, the confinement promotes the stability of the Saturn ring configuration. This study helps us to understand the existing experimental observations for confined systems where the metastablity of the Saturn ring is shown to be influenced by the presence of confining surfaces.

ACKNOWLEDGMENTS

This work was supported by the National Science Foundation through the University of Wisconsin's MRSEC on Nanostructured Interfaces.

[1] P. Poulin, H. Stark, T.C. Lubensky, and D.A. Weitz, Science **275**, 1770 (1997).
[2] P. Poulin and D.A. Weitz, Phys. Rev. E **57**, 626 (1998).
[3] T.C. Lubensky, D. Pettey, N. Currier, and H. Stark, Phys. Rev. E **57**, 610 (1998).
[4] R.W. Ruhwandl and E.M. Terentjev, Phys. Rev. E **55**, 2958 (1997).
[5] B.I. Lev and P.M. Tomchuk, Phys. Rev. E **59**, 591 (1999).
[6] E.M. Terentjev, Phys. Rev. E **51**, 1330 (1995).
[7] P. Poulin, V. Cabuil, and D.A. Weitz, Phys. Rev. Lett. **79**, 4862 (1997).
[8] J. Chen, P.J. Bos, H. Vithana, and D.L. Johnson, Appl. Phys. Lett. **67**, 2588 (1995).
[9] V.K. Gupta and N.L. Abbott, Science **276**, 1533 (1997).
[10] O.V. Kuksenok, R.W. Ruhwandl, S.V. Shiyanovskii, and E.M. Terentjev, Phys. Rev. E **54**, 5198 (1996).
[11] D. Andrienko, G. Germano, and M.P. Allen, Phys. Rev. E **63**, 041701 (2001).
[12] H. Stark, Eur. Phys. J. B **10**, 311 (1999).
[13] R.W. Ruhwandl and E.M. Terentjev, Phys. Rev. E **56**, 5561 (1997).
[14] H. Yokoyama, J. Chem. Soc., Faraday Trans. 2 **84**, 1023 (1988).
[15] M.M. Witterbrood, D.H. Luijendijk, S. Stallinga, and Th. Rasing, Phys. Rev. E **54**, 5232 (1996).
[16] P. Sheng, Phys. Rev. Lett. **37**, 1059 (1976); Phys. Rev. A **26**, 1610 (1982).
[17] T.J. Sluckin and A. Poniewierski, Liq. Cryst. **2**, 281 (1987).
[18] M.M. Telo da Gama and P. Tarazona, Phys. Rev. A **41**, 1149 (1990); M.M. Telo da Gama, P. Tarazona, M.P. Allen, and R. Evans, Mol. Phys. **71**, 801 (1990).
[19] B. Jérôme, Rep. Prog. Phys. **54**, 391 (1991).
[20] Y. Gu and N.L. Abbott, Phys. Rev. Lett. **85**, 4719 (2000).
[21] P.G. de Gennes and J. Prost, *The Physics of Liquid Crystals*, 2nd ed. (Clarendon Press, Oxford, 1993).
[22] A. Rapini and M. Papoular, J. Phys. (Paris), Colloq. **30**, C4 (1969).
[23] N. Schophol and T.J. Sluckin, Phys. Rev. Lett. **59**, 2582 (1987).
[24] E.H. Twizell, *Computational Methods for Partial Differential Equations* (Halsted Press, New York, 1984).
[25] H. Stark, J. Stelzer, and R. Bernhard, Eur. Phys. J. B **10/3**, 515 (1999).
[26] W.H. Press, S.A. Teukolsky, W.T. Vetterling, and B.P. Flannery, *Numerical Recipes* (Cambridge University Press, Cambridge, England, 1992).
[27] M. Kléman, *Points, Lines and Walls: In Liquid Crystals, Magnetic Systems, and Various Ordered Media* (Wiley, New York, 1983).